Inelastic x-ray scattering studies of low-energy charge excitations in graphite

N. Hiraoka,* H. Ishii, I. Jarrige, and Y. Q. Cai†
National Synchrotron Radiation Research Center, Hsinchu 30076, Taiwan
(Received 15 March 2005; published 1 August 2005)

We have studied charge excitations in graphite using inelastic x-ray scattering. The spectra were measured as a function of the momentum transfer, q, along the [100] (k_x), [210] (k_y), and [001] (k_z) axes on a high-quality single-crystal sample. Anisotropic and periodic features representing the semimetallic electronic structure have been observed. These features are interpreted based on band structure obtained from the local density approximation. On the $q \| k_x$ and $q \| k_y$ spectra, periodic signals exhibiting the gap opening and closing of the π bands have been observed. On the other hand, on $q \| k_z$ spectra, a forbidden excitation between the π bands has been detected in the high q region.

DOI: 10.1103/PhysRevB.72.075103 PACS number(s): 81.05.Uw, 81.07.−b, 73.90.+f, 78.70.Ck

I. INTRODUCTION

Graphite is an important, fundamental material in understanding the electronic structures of various technological materials. The crystal is obtained by ABA-type stacking of carbon layers having the honeycomb structure. Three electrons in $2s$ and $2p$ orbitals make up the $(sp_2)^3$ orbitals due to hybridization, and form strong covalent bonds in the c plane. The other electron occupies the weakly bonding $2p$ π orbitals and produce the conduction bands. This is the basic electronic structure of carbon-based materials (e.g., the nanotubes).[1] Furthermore, it has been discovered that nanostructured graphite stores a considerable amount of hydrogen atoms.[2,3] Graphite also has a crystal structure and a band structure similar to MgB_2 (see, e.g., Ref. 4), which has been found to show superconductivity with high critical temperature.[5] In addition, graphite continues to draw active interest in areas such as (i) unconventional transport properties under a magnetic field,[6] (ii) transformation to a superhard form under high pressure,[7] (iii) possible ferromagnetism,[8] etc.

Inelastic x-ray scattering (IXS), which has become popular since the recent advent of intense synchrotron radiation sources, is a useful technique to elucidate the excitation properties of materials. IXS covers a wide range of energy transfer ($\omega = E - E_0$) of $10^0 - 10^3$ eV with a single experimental setup. Furthermore, it measures excitation spectra as a function of momentum transfer (q) to the sample. The intensity of scattered x rays, namely the scattering cross section, is given by (see, e.g., Ref. 9):

$$\frac{d^2\sigma}{d\Omega d\omega} \propto -\hbar q^2/(4\pi^2 e^2 n)\mathrm{Im}[1/\varepsilon(q,\omega)], \qquad (1)$$

where ε is the dielectric function, $\hbar$ the Planck's constant, e the electron charge, and n the electron density. Similar information is obtained by electron energy loss spectroscopy (EELS). EELS has an excellent spatial resolution. However, its application to the high q range is limited by multiple scattering. In contrast, IXS has much less multiple scattering contribution. Furthermore, it has higher intensity at higher q due to the q^2 factor, although its intensity becomes rather weak at low q. The q range of IXS easily covers typical sizes of Brillouin zones. Therefore IXS is complementary to EELS. The energy resolutions of IXS have become comparable to those of EELS or even higher due to recent improvements. IXS was already applied to highly oriented pyrolytic graphite (HOPG) 17 years ago by Schülke *et al.*[10,11] It was however impossible to detect in-plane anisotropy since the HOPG sample does not have any in-plane long range order. Moreover, the limited resolution made findings of low-energy excitation features difficult because those features were hidden under the tail of the broad elastic line. EELS has also been applied to graphite several times so far.[12,13] They revealed in-plane anisotropy, but information concerning the relation between the signals and the lattice periodicity was limited due to the small q range.

In this article, we show IXS spectra measured as a function of q on a high quality single crystal. Low-energy excitation features have been detected due to improved resolution. We discuss the anisotropic, periodic signals of $\pi \rightarrow \pi^*$ transitions observed in in-plane spectra. We also discuss signals of $\pi \rightarrow \pi^*$ forbidden transitions, observed in on-axis spectra in high q. These are newly found excitation features that the previous IXS and EELS experiments did not detect. Furthermore the origin of several prominent features on the IXS spectra is elucidated based on previous theoretical studies.[14,15]

II. EXPERIMENT

The sample was a single crystal having a size of $\sim 2 \times 2 \times 0.1$ mm^3. Typically, the carbon layers in graphite are easily oriented along the c axis but not along the other axes (HOPG sample). Our sample showed clear diffraction spots on Laue photographs, indicating that the layers were oriented in the c plane as well. The experiments were carried out on the Taiwan inelastic x-ray scattering beamline (BL12XU) at SPring-8.[16] The synchrotron radiation from an undulator was monochromated by a Si111 double-crystal monochromator. The bandwidth of the beam was reduced to ~ 140 meV by four Si400 crystals placed after the monochromator. The beam was then focused into a 120×80 μm^2 spot on the sample by a Pt-coated Si focusing mirror. The scattered x rays were monochromated ($E_0 = 9883$ eV), collected by an analyzer system, and finally detected by a Si diode. The spectra were recorded up to $E - E_0 = 80$ eV by scanning the

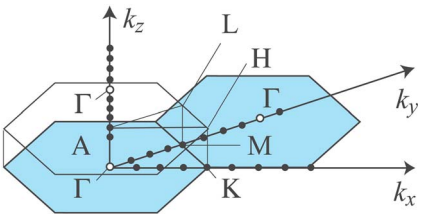

FIG. 1. (Color online) q points on which the IXS spectra were measured (filled circles). IXS measurements were not possible on Γs (open circles) because the Bragg reflections were too intense.

incident photon energy (E) from 9883 to 9963 eV. The total energy resolution was ~180 meV while the q resolution was ~2.0 nm^{-1} along the scattering plane.[25] The IXS spectra were measured at 8 or 9 q points along the [100] (k_x), [210] (k_y) and [001] (k_z) axes. The positions of q's are summarized in Fig. 1, and the values are shown in Fig. 2 with the raw spectra. Most of the spectra were measured by a multianalyzer system, where three Si555 spherical crystals were positioned along the vertical axis, i.e., a line perpendicular to the scattering plane. The multianalyzer system improves count rates, but it substantially deteriorates the angular resolution along the vertical direction in low q. For this reason, the spectra were measured with a single analyzer for k_x =4.2 nm^{-1}, k_y=3.7 nm^{-1}, and $k_z \leqslant 8.2$ nm^{-1}. The experiments were carried out at room temperature.

The background was evaluated to be 0.050 counts per second by tilting the analyzers away by 0.2° so as to eliminate the real signals. The signals from elastic scattering were negligible for the in-plane spectra in $E-E_0 \geqslant 1.6$ eV, but small contributions were found for the on-axis spectra up to ~4 eV. Assuming the tails to be inversely proportional to $E-E_0$, we subtracted the tails and the constant background from the spectra before computing the dielectric functions.

III. RESULTS AND DISCUSSIONS

A. Plasmon dispersions

Figure 2 shows the raw spectra, which are corrected only for the intensity of the incident beam. The small peaks at ~7 eV at $1/12\text{-}G_x$ and at $1/8\text{-}G_y$ arise from the so-called π plasmon, while the large peaks at ~28 eV correspond to the $\sigma+\pi$ plasmon. They show anisotropy and large q dispersions. The π plasmon peak monotonically shifts to the high energy side with increasing q along k_x, while it looks as if it had split into two (or more) peaks around the $3/8G_y$. In order to have a closer insight, we have computed the dielectric functions using the sum rule (see, e.g., Ref. 10) and the Kramers–Kronig transformation.[17] The lower panels in Fig. 2 show the real part (ε_1) and the imaginary part (ε_2) of the dielectric function. The sum rule is given by $\int \mathrm{Im}[1/\varepsilon]\omega d\omega = -2\pi^2 e^2 n/m$. According to this equation, the dielectric functions provide smaller (absolute) values at higher q for the in-plane spectra, which rapidly become broad as q increases, shifting their spectral weights to the

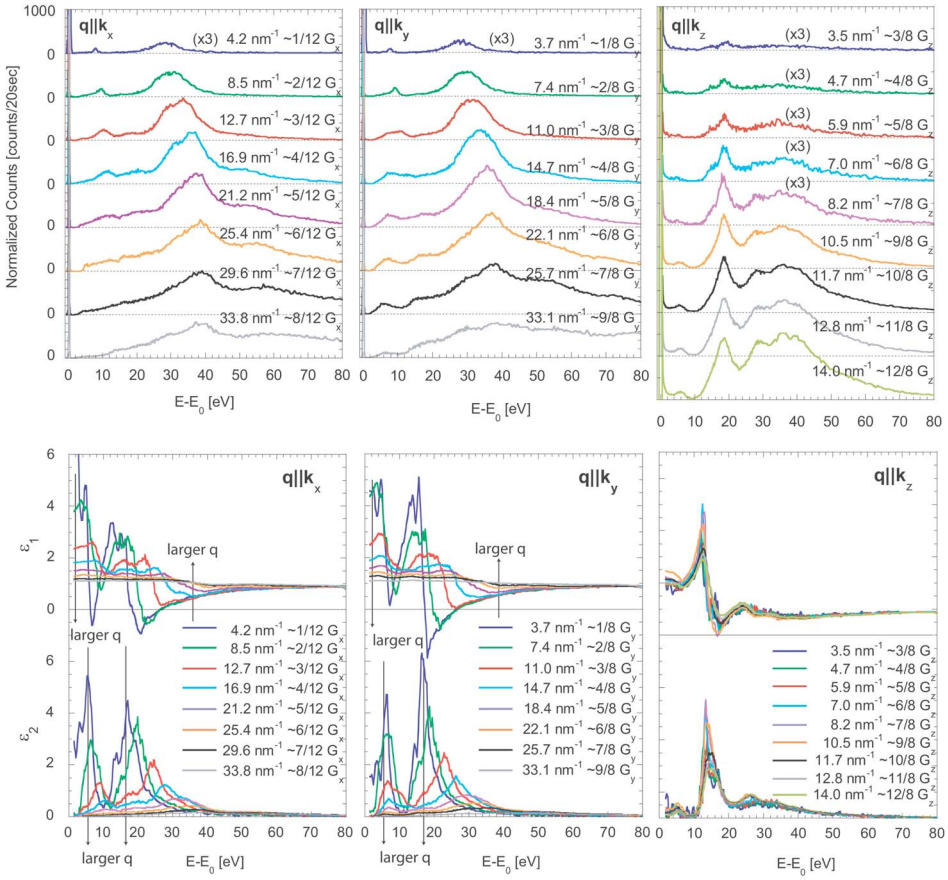

FIG. 2. (Color online) Raw spectra and dielectric functions.

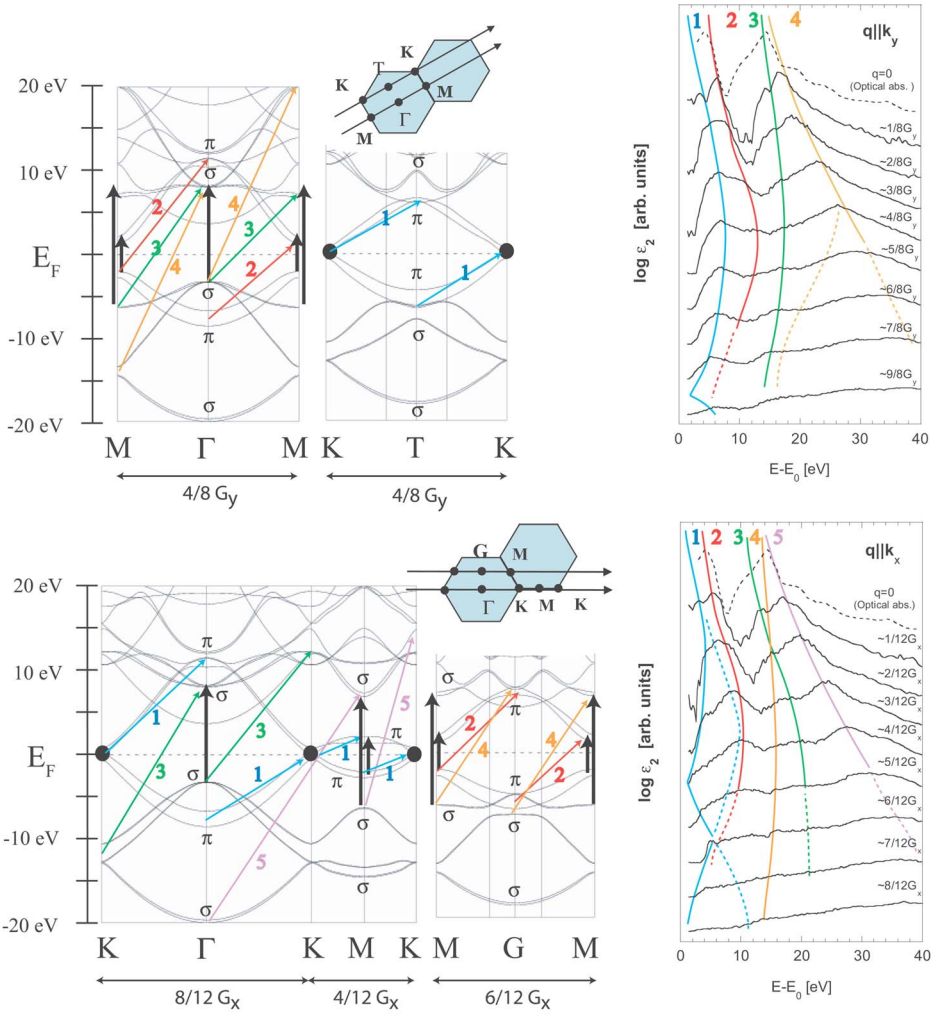

FIG. 3. (Color online) In-plane dielectric functions (imaginary parts) and associated band-structure diagrams. The dielectric functions obtained from the optical study ($q=0$) on a HOPG sample, Ref. 22, are replotted with dashed curves. The logarithm is taken for each curve so as to emphasize low-intensity signals. Thick (vertical) arrows indicate transitions having strong oscillator strength, as reported in Ref. 14.

high energy side. Since the spectra are normalized based on the sum rule, which is independent of q, the dielectric functions at low q are noisier due to the weaker intensities in the raw spectra. However, it has been confirmed that these dielectric functions are quite similar to those in a previous IXS experiment[10] and in a theoretical study.[14] In low q, the dielectric function along k_x and k_y shows a plasmon-like behavior near 6 eV: Namely, the real part becomes zero (or almost zero) while the imaginary part has a small value. This feature is already lost at $\sim 10.0\ \mathrm{nm}^{-1}$. This implies disappearance of the plasmon and domination of the spectra by interband transitions. In order to understand the IXS spectra, it is essential to clarify the origin of each feature based on the band structure.

B. In-plane excitations

We first discuss the $q \| k_y$ dielectric functions for the sake of simplicity. Figure 3 shows the imaginary parts of the dielectric functions for $q \| k_y$ spectra, along with the associated band structure diagrams. Generally, dielectric functions do not display any peak structure for collective excitations (plasmons). Therefore, peak structures found on those curves should be ascribed to intra- or interband transitions. These functions are the same as those in Fig. 2, but the logarithm is taken to highlight low-intensity features, and also each curve is shifted in the vertical axis so as to clarify the q evolution. Furthermore, the dielectric function from an optical study ($q=0$) on a HOPG sample, Ref. 22, is replotted in the figure with a dashed curve for comparison with our IXS data. The band structure was calculated using the full-potential linearized augmented plane-wave method (FLAPW) based on the local density approximation (LDA).[24,26] The obtained band structures are very similar to those in a previous report.[14] It is often argued that LDA band structures cannot be directly compared with optical absorption, EELS or IXS spectra, because the band structure are not meant to describe *excited* states.[13,14,18,19] However, as seen in Ref. 14, it is straightforward to understand the optical absorption spectra of graphite based on the band structure diagram. This fact justifies the comparison between the IXS spectra and the band structure, at least, for qualitative discussions.

Four branches are discernible in the dielectric functions, as numbered from 1 to 4 in the Fig. 3 (upper panel). The band structure of graphite has already been discussed in previous theoretical reports,[14,15] based on optical absorption[20–23] and EELS (low-q)[12] data. The following two major transitions have been pointed out: (i) Intraband transitions of π conduction electrons at K, marked by the solid circles in Fig. 3, and (ii) the $\pi \rightarrow \pi^*$ ($\sim$5 eV) and the $\sigma \rightarrow \sigma^*$ ($\sim$14 eV) transitions at Γ and M, marked by thick (vertical) arrows. It is important to mention that $\pi \rightarrow \pi^*$ and $\sigma \rightarrow \sigma^*$ transitions are allowed for in-plane excitations, due to the almost two-dimensional band structure.[10,14] It is reasonable to assume that prominent features in IXS spectra ($q \neq 0$) share either the initial or the final state of the $q=0$ transitions, which have large oscillator strength in the optical absorption. Based on this assumption, we determine the origins of the four branches. The first branch approaches $E-E_0=0$ eV as $q \rightarrow 0$ or G_y, where G_y is the first reciprocal lattice vector along k_y or [210]. It is therefore clear that this is due to the $\pi \rightarrow \pi^*$ transitions along the K-T-K axes. The second branch shows $E-E_0 \sim 5$ eV at low q. Hence this is ascribed to the $\pi \rightarrow \pi^*$ transition along the M-Γ-M. The turning back of this branch is invisible in high q. This is probably because of the less-defined dipole approximation in this region. The third branch always remains between 14 and 16 eV and has a small dispersion. It is explained by transitions between the heavy σ bands along the M-Γ-M. The fourth branch starts from $\sim$16 eV at $1/8G_y$ and shows a very large dispersion. This might represent the transitions between the light σ bands along the M-Γ-M. However, the electron-hole pair excitation process generally dominates in such a high q, high E region.[9] Since its signal also rapidly moves to the high energy side as q increases, we suspect these interband excitations are combined with the electron-hole pair excitation, smearing out the structures in the spectra.

Although the $q \| k_x$ spectra should be interpreted in a similar way, it appears more difficult to follow each q evolution than for the $q \| k_y$ ones. That is because the $\pi \rightarrow \pi^*$ or $\sigma \rightarrow \sigma^*$ transitions, having large oscillator strength at M, K, or Γ (thick arrows), can have more complicated evolutions (see Fig. 3, lower panel). The first branch is prominent only at low energy. This branch approaches 0 eV at $q \sim 0$, 4/12, and $8/12G_x$, where G_x is the first reciprocal lattice vector along k_x or [100]. It is clear that this represents the $\pi \rightarrow \pi^*$ transition along the K-Γ-K-M-K. Comparing with the band structure diagram, we notice that this branch actually consists of two sets of $\pi \rightarrow \pi^*$ transitions, i.e., those along the K-Γ-K and those along the K-M-K, as marked with a dashed curve. Our interpretation for the other excitations is shown on the figure. In order to clarify their origin, it is necessary to calculate the dielectric function based on accurate theories, e.g., the time-dependent density functional theory.[18,19] Such a calculation would allow more quantitative discussions.

C. On-axis excitations

Figure 4 shows the imaginary parts of the dielectric functions obtained from the $q \| k_z$ IXS spectra and the associated band structure diagrams. The dielectric function from the optical study Ref. 22 ($q=0$), replotted with the dashed curve in the figure, shows abrupt shifts of the peak positions, compared with the $q \neq 0$ ones. We believe this is due to errors in the optical study, where the exact on-axis geometry was not achieved in the experiments. In fact, the theoretical dielectric function for $q=0$[14] is rather close to our IXS ones at low q.

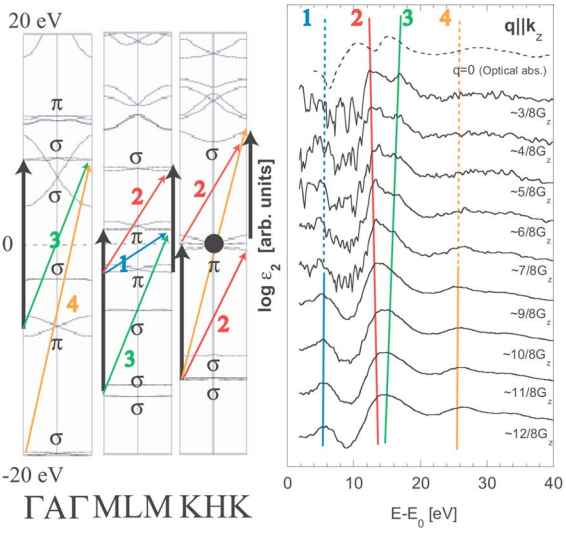

FIG. 4. (Color online) On-axis dielectric functions (imaginary parts) and associated band-structure diagrams. The dielectric function obtained from the optical study, Ref. 22 ($q=0$), is replotted with a dashed curve. The logarithm is taken for each curve so as to emphasize low-intensity signals. Thick (vertical) arrows indicate the transitions having strong oscillator strength, as reported in Ref. 14.

Unlike in-plane transitions, on-axis ones show very small dispersions. Four branches are discernible in the dielectric functions, as numbered from 1 to 4 in the figure. The most interesting branch is at $\sim$5 eV, which is enhanced at high q. Because of the almost two-dimensional electronic structure, $\pi \rightarrow \sigma^*$ and $\sigma \rightarrow \pi^*$ transitions are allowed for $q \| k_z$.[10,14] Therefore, this branch is ascribed to the nondipole transitions between the π bands along the M-L-M axes with large q. The second and the third branches are believed to originate from $\pi \rightarrow \sigma^*$ or $\sigma \rightarrow \pi^*$ transitions, as already reported in a previous IXS experiment.[10] The fourth branch at $\sim$26 eV only appears at high q, similarly to the first branch. The possible transition is the $\sigma \rightarrow \sigma^*$ forbidden transition, which happens in the entire Brillouin zone.

IV. SUMMARY

The IXS spectra were measured as a function of q along the k_x ([100]), k_y ([210]), and k_z ([001]) directions. The structures on the spectra and their q evolutions were understood based on the LDA band structure. Clear q evolutions were observed for the charge excitations of $\sim$5 eV, representing the semimetallic electronic structure. For $q \| k_x$ and $q \| k_y$, periodic features exhibiting gap opening and closing were observed, whereas for $q \| k_z$, the $\pi \rightarrow \pi^*$ forbidden excitations were detected in high q.

ACKNOWLEDGMENTS

We thank A. Chainani for stimulating discussions and a critical reading of the manuscript. We are grateful to C. C. Chen for technical support, and to D. J. Wang and S. Y. Perng for preparing the analyzer crystals for the experiments. We would also like to thank Professor Suematsu for providing us with the sample. The work was carried out at SPring-8 under Experiment No. C04B12XU-1510N, and was partly supported by NSRRC and NSC of Taiwan.

*Electronic address: hiraoka@spring8.or.jp
†Electronic address: cai@spring8.or.jp

[1] S. Iijima, Nature (London) **354**, 56 (1991).
[2] S. Orimo, G. Majer, T. Fukunaga, A. Züttel, L. Schlapbach, and H. Fujii, Appl. Phys. Lett. **75**, 3093 (1999).
[3] S. Orimo, T. Matsushima, H. Fujii, T. Fukunaga, and G. Majer, J. Appl. Phys. **90**, 1545 (2001).
[4] J. M. An and W. E. Pickett, Phys. Rev. Lett. **86**, 4366 (2001).
[5] J. Nagamatsu, N. Nakagawa, T. Muranaka, Y. Zenitani, and J. Akimitsu, Nature (London) **410**, 63 (2001).
[6] X. Du, S. W. Tsai, D. L. Maslov, and A. F. Hebard, Phys. Rev. Lett. **94**, 166601 (2005).
[7] W. L. Mao, H. K. Mao, P. J. Eng, T. P. Trainor, M. Newville, C. C. Kao, D. L. Heinz, J. Shu, Y. Meng, and R. J. Hemley, Science **302**, 425 (2003).
[8] P. Esquinazi, A. Setzer, R. Höhne, C. Semmelhack, Y. Kopelevich, D. Spemann, T. Butz, B. Kohlstrunk, and M. Lösche, Phys. Rev. B **66**, 024429 (2002).
[9] W. Schülke, J. Phys.: Condens. Matter **13**, 7557 (2001), and references therein.
[10] W. Schülke, U. Bonse, H. Nagasawa, A. Kaprolat, and A. Berthold, Phys. Rev. B **38**, 2112 (1988).
[11] W. Schülke, A. Berthold, A. Kaprolat, and H. J. Güntherodt, Phys. Rev. Lett. **60**, 2217 (1988).
[12] U. Büchner, Phys. Status Solidi B **81**, 227 (1977).
[13] A. G. Marinopoulos, L. Reining, V. Olevano, A. Rubio, T. Pichler, X. Liu, M. Knupfer, and J. Fink, Phys. Rev. Lett. **89**, 076402 (2002).
[14] A. G. Marinopoulos, L. Reining, A. Rubio, and V. Olevano, Phys. Rev. B **69**, 245419 (2004).
[15] A. Grüneis, R. Saito, G. G. Samsonidze, T. Kimura, M. A. Pimenta, A. Jorio, A. G. SouzaFilho, G. Dresselhaus, and M. S. Dresselhaus, Phys. Rev. B **67**, 165402 (2003).
[16] Y. Q. Cai, P. Chow, C. C. Chen, H. Ishii, K. L. Tsang, C. C. Kao, K. S. Liang, and C. T. Chen, AIP Conf. Proc. **705**, 340 (2004).
[17] G. W. Milton, D. J. Eyre, and J. V. Mantese, Phys. Rev. Lett. **79**, 3062 (1997).
[18] L. Reining, V. Olevano, A. Rubio, and G. Onida, Phys. Rev. Lett. **88**, 066404 (2002).
[19] S. Botti, Phys. Scr., T **109**, 54 (2004).
[20] E. A. Taft and H. R. Philipp, Phys. Rev. **138**, A197 (1965).
[21] L. G. Johnson and G. Dresselhaus, Phys. Rev. B **7**, 2275 (1973).
[22] R. Klucker, M. Skibowski, and W. Steinmann, Phys. Status Solidi B **65**, 703 (1974).
[23] M. Hanfland, K. Syassen, and R. Sonnenschein, Phys. Rev. B **40**, 1951 (1989).
[24] M. Umekawa, N. Hamada, A. Kodama, and Y. Moritomo, J. Phys. Soc. Jpn. **73**, 430 (2004).
[25] Spectra at 4.2 nm^{-1} on the k_x and 3.7 nm^{-1} on the k_y were measured with a resolution of 250 meV for higher count rates using a different analyzer crystal.
[26] Calculated by the MIZUHO-ABCAP code (Ref. 24).